Structural and ferromagnetic properties of Cu-doped GaN

B. Seipel[a)]
Department of Physics, Portland State University, Portland, Oregon 97207-0751; and Oregon Nanoscience and Microtechnologies Institute (ONAMI)

R. Erni[b)]
Department of Chemical Engineering and Materials Science, University of California at Davis, Davis, California 95616

Amita Gupta
Department of Physics, Portland State University, Portland, Oregon 97207-0751; Department of Materials Science, Tmfy-MSE, The Royal Institute of Technology, SE 100 44 Stockholm, Sweden; and National Center for Electron Microscopy, Lawrence Berkeley National Laboratory, Berkeley, California 94720

C. Li
Department of Physics, Portland State University, Portland, Oregon 97207-0751; and Oregon Nanoscience and Microtechnologies Institute (ONAMI)

F.J. Owens
Army Armament Research, Development and Engineering Center, Picatinny, New Jersey 07896; and Department of Physics, Hunter College, City University of New York, New York 10024

K.V. Rao
Department of Materials Science, Tmfy-MSE, The Royal Institute of Technology, SE 100 44 Stockholm, Sweden

N.D. Browning[c)]
Department of Chemical Engineering and Materials Science, University of California at Davis, Davis, California 95616; and National Center for Electron Microscopy, Lawrence Berkeley National Laboratory, Berkeley, California 94720

P. Moeck
Department of Physics, Portland State University, Portland, Oregon 97207-0751 and Oregon Nanoscience and Microtechnologies Institute (ONAMI)

(Received 24 October 2006; accepted 15 February 2007)

The wurtzite polymorph of GaN was calcined with CuO in flowing nitrogen. As a result of this processing, both superconducting quantum interference device magnetometry and ferromagnetic resonance studies showed ferromagnetism in these samples at room temperature. These magnetic results are qualitatively consistent with very recent first-principle calculations [Wu et al., *Appl. Phys. Lett.* **89,** 062505 (2006)] that predict ferromagnetism in Cu-doped GaN. We focus in this paper on analyzing changes in the GaN atomic and electronic structure due to calcination with CuO using multiple analytical methods. Quantitative powder x-ray diffraction (XRD) showed changes in the lattice constants of the GaN due to the incorporation of copper (and possibly oxygen). Energy-dispersive x-ray spectroscopy proved the incorporation of copper into the GaN crystal structure. Electron-gun monochromated electron energy loss spectroscopy showed CuO calcinations-induced GaN band gap changes and indicated changes in the atomic arrangements due to the calcination process. The fine structure of the N K-edge showed differences in the peak ratios with respect to higher nominal CuO contents, corresponding to an increase in the *c*-lattice constant as confirmed by XRD.

[a)]Address all correspondence to this author.
e-mail: bseipel@pdx.edu
[b)]Present address: EMAT, University of Antwerp, Groenenborgerlaan 171, B-2020 Antwerp, Belgium
[c)]Present address: Materials Science and Technology Division, Chemistry and Materials Science Directorate, Lawrence Livermore National Laboratory, Livermore, CA 94550
DOI: 10.1557/JMR.2007.0168

I. INTRODUCTION

Ferromagnetic semiconductors (i.e., a special class of spintronics materials) with Curie temperatures (T_C) at and above room temperature have the potential to add new functionality to established microelectronics.[1,2] Prospective candidates are dilute (d) magnetic semiconductors (DMSs) that are synthesized by doping conventional

semiconductors with transition metals (TMs), e.g., Fe, Co, Ni, Cr, or Cu.[3,4]

DMSs have found enormous interest in the scientific community after the year 2000 when theoretical work by Dietl and co-workers was published.[5] Those authors predicted ferromagnetism above room temperature in Mn-doped ZnO and GaN. Ferromagnetism is predicted to occur through interactions between the local magnetic moments of the TM cations that are mediated by free holes. Very recent spin density functional theory (DFT) calculations by Wu and co-workers predict spin polarization of Cu when it is incorporated into GaN.[6] This spin polarization is predicted to magnetize p electrons of the tetrahedrally coordinated N atoms through p-d hybridization, which leads to a ferromagnetic coupling of the Cu dopants at a T_C above 350 K and a magnetization of 0.125 Bohr magneton per Cu dopant.

On the experimental side, Sharma et al.[7] did indeed find ferromagnetism above room temperature in Mn-doped ZnO, confirming the predictions by Dietl et al.[5] This observation has been substantiated by various reports that include magnetic circular dichroism measurements as well as magneto-transport and magneto-optical studies.[8–10] At present, ferromagnetism above, at, or slightly below room temperature has been reported in wurtzite-type semiconductors for Mn-doped,[11–13] Cr-doped,[14] and Gd-doped[15] gallium nitride as well as for Mn-doped,[7,16,17] Fe-doped,[18] Co-doped,[19–21] Ni-doped,[22] and Cu-doped[23,24] zinc oxide. The latter case deserves some further discussion, because ZnO and GaN may be straightforwardly compared since both semiconductors possess the wurtzite structure with similar lattice constants (a = ~0.32 nm and c = ~0.52 nm), and both have direct band gaps of similar widths (~3.4 eV).[25]

Feng predicted ferromagnetism in Cu-doped ZnO.[26] Possible clusters of Cu, CuO, and Cu_2O would not be ferromagnetic.[27,28] Wahl et al. reported that the copper atoms are primarily located at the cation sites (of the wurtzite structure) when ZnO is doped with Cu.[29] For Cu ordering primarily along the crystallographic c-axis, i.e., the so-called "far"-model with a Cu–Cu distance of 0.5205 nm, a ferromagnetic ground state was predicted.[26] Additional hole doping was assumed to be crucial for the stabilization of this ferromagnetism.[26] Buchholz et al. reported ferromagnetism in Cu-doped ZnO thin films above room temperature for growth in a nitrogen-rich atmosphere, providing the required additional p-type carriers for ferromagnetism to occur.[23]

Despite all enthusiasm about the reported ferromagnetism in ZnO- and GaN-based DMSs, there are still complexities in verifying the mechanisms responsible for its occurrence. This has led to controversial discussions about the origin of the ferromagnetism, even suggesting that the observed magnetic properties could be that of a "pseudo-DMS" due to clusters of magnetic atoms, other impurities, or precipitated phases. For example, P. Bogusławski and J. Bernholc showed that the segregation of Mn to form MnN clusters is favorable in Mn-doped GaN.[30] Fortunately, those authors also showed that both pseudomorphic or structurally relaxed MnN would be antiferromagnetic.[30] Ferromagnetism was also observed in TM doped n-type nitrides and oxides[31,32] (in disagreement with Dietl's and coworkers' predictions[5]), and the bound magnetic polaron model (indirect exchange via shallow donors)[31,32] was proposed as explanation. N-type doping of GaN may result unintentionally from impurities such as oxygen.

At present, there are, to the best of our knowledge, no published experimental observations (other than those in our conference proceedings papers) on ferromagnetism in Cu-doped GaN. This first archival journal paper reports on structural and electronic effects of CuO calcination on GaN powders that led to ferromagnetism at room temperature. The exact source of this ferromagnetism has so far not been elucidated experimentally, but is very likely to be due to Cu incorporation into the GaN. More elaborate processing and characterization studies, involving thin films, are in progress to identify the origin of the observed ferromagnetism and will be published elsewhere.

II. EXPERIMENTAL DETAILS

GaN powders (nominal purity 99.999%) were mixed with 2, 4, 6, and 8 wt% CuO powders (nominal purity 99.9999%) by grinding them with mortar and pestle; see Table I for the sample names and nominal compositions. The mixtures were compressed into pellets and calcined for 4 h at 773 K in flowing nitrogen at The Royal Institute of Technology in Stockholm.[24] The pellets were then allowed to cool down to room temperature in nitrogen. Subsequently, the pellets were crushed with mortar and pestle for the analyses we describe in this paper. A reference GaN sample (from the same supplier) without any added CuO was heat treated in exactly the same manner (reference sample G0, Table I).

Superconducting quantum interference device (SQUID) measurements were performed at The Royal Institute of Technology in Stockholm[24] employing a Quantum Design (San Diego, CA) MPMS-2 instrument. Ferromagnetic resonance (FMR) measurements were performed at the Army Armament Research, Development and

TABLE I. Sample names and nominal constituents.

Sample name	Nominal sample constituents
G0	GaN
G2	GaN + 2 wt% CuO
G4	GaN + 4 wt% CuO
G6	GaN + 6 wt% CuO
G8	GaN + 8 wt% CuO

Engineering Center in Picatinny using a Varian E-9 (Varian, Inc., Palo Alto, CA) electron paramagnetic resonance spectrometer operating at 9.2 GHz. Further details of such measurement are described elsewhere.[24,33]

For quantitative powder x-ray diffraction (XRD) studies at Portland State University (PSU), the samples were mixed with a silicon standard at a ratio 10 GaN to 1 Si (as derived from wt%). Powder XRD diffractograms were recorded between 20° and 100° 2θ with a Philips X'Pert (PANalytical B.V. Lelyweg 1, Almelo, The Netherlands) PW3040 (employing Cu $K_{\alpha\ 1/2}$ radiation, a step size of 0.02 2θ, counting 10 s/step, using a 5 mm slit and an energy-dispersive Peltier-cooled detector). The Powder Diffraction File (PDF-2, release 1999) database of the Joint Committee on Powder Diffraction Standards (JCPDS) was used for the qualitative phase determination. The average lattice constants of the GaN in all samples were quantified by means of the Rietveld method, employing one of the freely available software packages.[34]

The samples were also examined with PSU's FEI (Hillsboro, OR) Tecnai G^2 F20 ST transmission electron microscope with scanning probe facility (TEM/STEM) operated at 200 kV and equipped with both an energy dispersive x-ray spectrometer (EDXS) and a Gatan Imaging Filter for electron energy loss spectroscopy (EELS) in the STEM mode.

More sophisticated EELS was performed at the National Center for Electron Microscopy (NCEM) at the Lawrence Berkeley National Laboratory (LBNL) using a gun-monochromated FEI Tecnai G^2 F20 UT microscope (STEM/TEM) operated at 200 kV. That microscope is equipped with a high-resolution post-column spectrometer (GIF Tridiem)[35] and a Wien-filter type electron monochromator.[36,37] This experimental setup allows for an energy resolution in EELS of 0.2 to 0.25 eV.[36] The EELS was carried out in the STEM mode, and fine-structure core-loss spectra as well as valence electron energy loss spectra (VEELS) were recorded with the electron energy monochromator switched on.

The (fine-grain powder) samples were in each case dispersed with propanol on Au grids (instead of the more popular Cu grids) since we intended to analyze effects of the incorporation of copper into the GaN grains. The grids were mounted on low-background double-tilt holders to minimize the non-specimen-related contributions to the EDX (and EEL) spectra.

III. RESULTS AND DISCUSSIONS

A. Magnetic measurements

We observed ferromagnetism at room temperature in all samples that were calcined with CuO. Figure 1 shows typical results of the SQUID measurements, i.e., magnetic moment per unit mass versus applied magnetic field

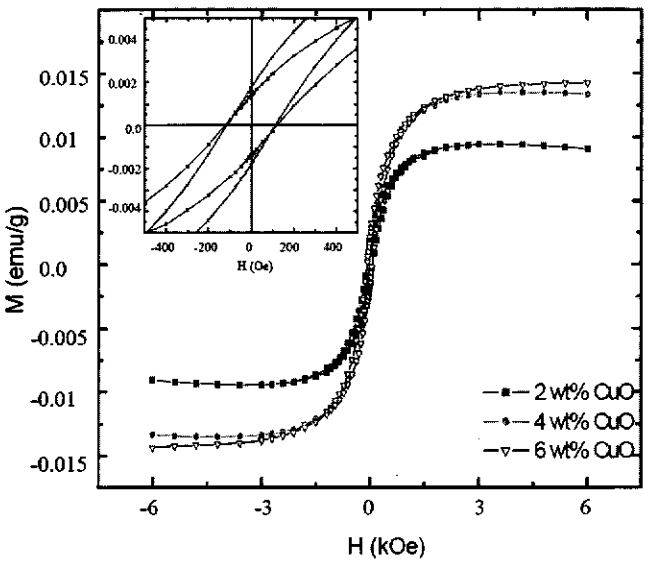

FIG. 1. Magnetic moment per unit mass (magnetization, M) versus applied magnetic field (H) hysteresis curves at 300 K for samples G2, G4, and G6. The inset shows the magnified section of the M versus H curves around zero magnetic field. The hysteresis curves for samples G4 and G6 fall almost on top of each other and are nearly indistinguishable in the inset. While coercive fields are of the order of 100 Oe, remnant magnetizations are of the order of 1.5×10^{-3} emu/g. The saturation magnetizations are approximately 1 order of magnitude higher (0.01 Bohr magneton per Cu atom) than the remnant magnetizations. (1 emu = 10^{-3} A m^2, 1 Oe = $10^3/4\pi$ A/m).

hysteresis curves, for samples G2, G4, and G6 at 300 K. The inset in Fig. 1 shows the remanent flux densities (remanences) and coercivities. The observed magnetic characteristics in Fig. 1, with low remanence and small magnetic coercivity are common observations found in many DMSs at room temperature. Note that the magnetic data shown in Fig. 1 is the "as-obtained" data, and no corrections for the "magnetic background," including possible contributions from the cellulose sample holder, possible diamagnetism from unreacted GaN, and the small paramagnetic term that arises from unreacted CuO, have been made.

These SQUID measurements confirm earlier FMR measurements on analogous powder samples with very similar compositions and calcination parameters. [Note that in a single crystal the field position of the ferromagnetic resonance depends on the orientation of the direct current (dc) magnetic field with respect to the coordinate system of the crystal. The spectra shown in this paper are from a collection of randomly oriented grains and are, therefore, "powder FMR spectra," representing the sum of spectra from all respective orientations of the dc magnetic field.] As characteristic for an intrinsic ferromagnetic material, those samples showed a broadening and shift of the magnetic resonance field line to lower fields as the temperature is decreased, e.g., Fig. 2. The temperature dependencies of the corresponding center of resonance line position and line widths of the FMR

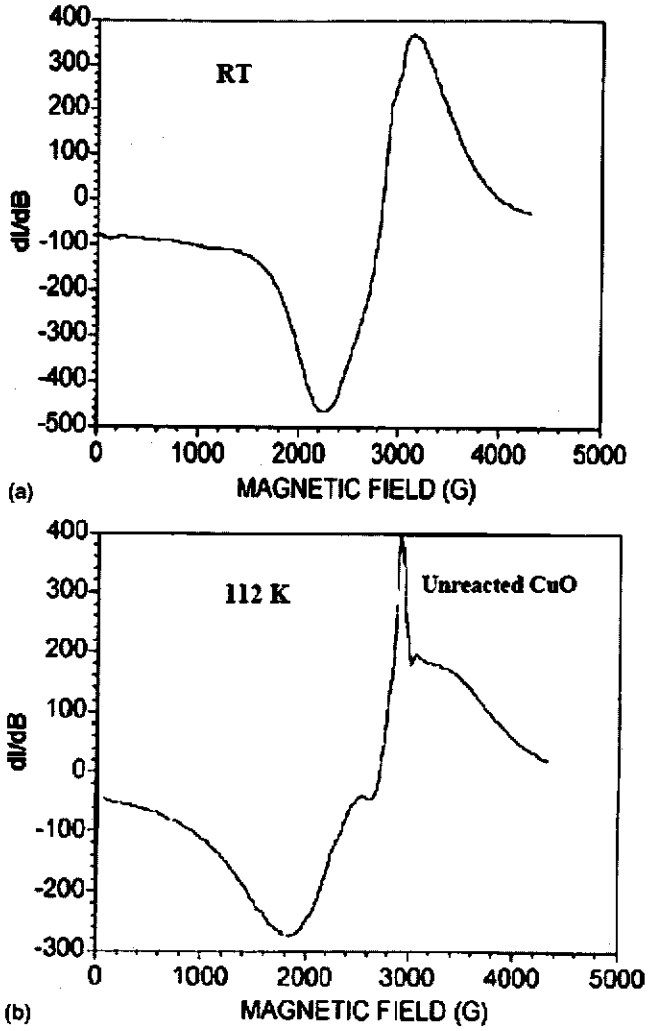

FIG. 2. (a) FMR spectra at 300 K (considered to be room temperature and abbreviated as RT and (b) 112 K for CuO-calcined GaN powders. The spectrum at 112 K shows the expected FMR peak broadening and shift of the center of the resonance with respect to the spectrum that was recorded at room temperature. The narrow line in the 112 K spectrum is likely to arise from unreacted (paramagnetic) CuO (1 G = 10^{-4} T).

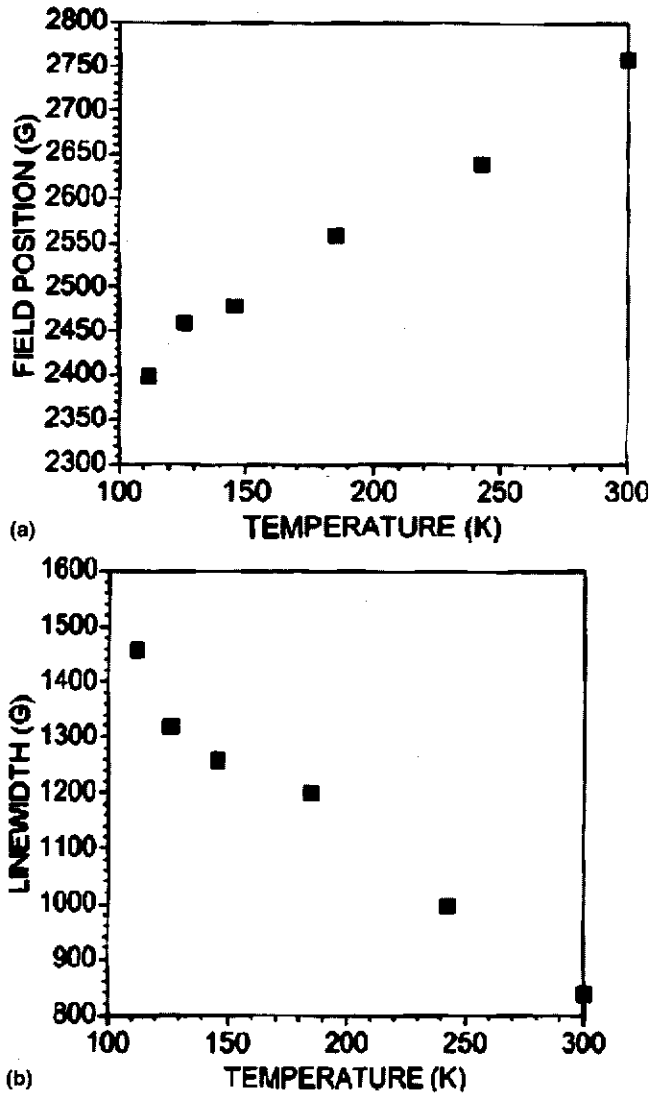

FIG. 3. (a) Temperature dependencies of the FMR center of resonance line and (b) line width for CuO-calcined GaN powders (1 G = 10^{-4} T).

signals are shown in Fig. 3. All of these FMR observations are analogous to those in other reports on ferromagnetic semiconductors[7,16,24] and support our conclusion that the CuO-calcined GaN powders are definitely ferromagnetic at room temperature. (It should be noted again that unreacted CuO cannot be the source of the observed ferromagnetism.) Our observations of room-temperature ferromagnetism in CuO-calcined GaN are qualitatively consistent with the results of Wu and co-workers' DFT calculations for 5.56 and 6.25 at.% Cu substitutionally incorporated in GaN that favor a ferromagnetic ground state.[6]

The observed remanence and the saturation magnetization were highest for sample G6 (although sample G8 contained nominally more CuO). The illustrations of the EDXS and EELS results that are presented below are, therefore, exclusively given from this sample (whereby the observed trends of our structural and spectroscopic analyses were generally the stronger the more CuO powder was added to the nominally pure GaN powder prior to the calcination with identical processing parameters).

It is significant that while all CuO-calcined samples showed room-temperature ferromagnetism, there was no evidence of ferromagnetism in the nominally pure GaN reference sample, G0. (Electron paramagnetic resonance measurements with a sensitivity to parts per 10 billion were also made on the GaN powders before CuO calcination and showed no evidence of the existence of magnetic impurities.) Again, we note that Cu, CuO, and Cu_2O are known to be not ferromagnetic at room temperature.[27,28]

B. X-ray diffraction analysis

In all samples that were calcined with CuO, we identified the following crystal phases: GaN, CuO, and Cu_2O. Figure 4 shows, for example, a section of the powder XRD diffractogram of sample G6 that contains the strongest peaks for all identified phases. The positions and relative intensities of the GaN triplet (32.5°, 34.7°, 37.0° 2θ, CuO peaks (35.5° 2θ and 38.7° 2θ), and the Cu_2O peak (36.5° 2θ) are in agreement with the JCPDS database.

The presence of Cu_2O after calcination (under flowing nitrogen) in samples G2, G4, G6, and G8 suggests that the reduction of copper in the oxides (i.e., Cu^{2+} to Cu^{+}) is due to the thermal treatment that accompanied the calcination processes. It is well known that CuO is not stable under low O_2 pressures at temperatures greater than 450 °C. Under such conditions, a disproportionation of the type

$$2 \cdot CuO_{solid} \rightarrow Cu_2O_{solid} + 0.5 \cdot O_{2\ gaseous} \quad , \qquad (1)$$

can take place.[38]

Figure 5 shows the average lattice constants of the GaN phases with respect to the nominal CuO content in the calcined powders. The *c*-lattice constant [Fig. 5(a)] increases with higher nominal CuO contents. Similarly, the *a*-lattice constants [Fig. 5(b)] show an increase with higher CuO contents as well, after an initial drop from the values of the nominally pure reference GaN sample. Because the reference GaN sample was subjected to the same heat treatment and gaseous environment as the CuO-calcined samples, it can be concluded that the changes in the lattice constants are due to changes in the GaN crystal structure (i.e., copper and/or oxygen incorporation into the wurtzite GaN structure).

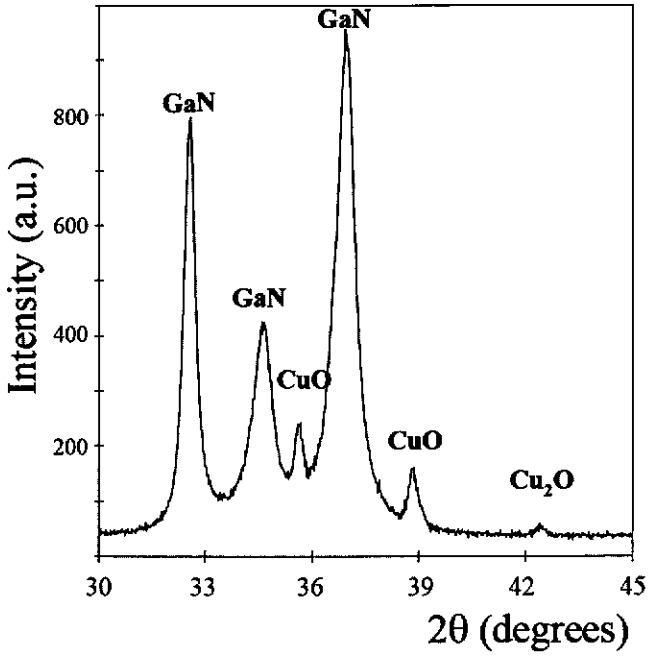

FIG. 4. Section of the powder x-ray diffractogram of sample G6 containing the strongest peaks of the identified phases (GaN, CuO, and Cu_2O).

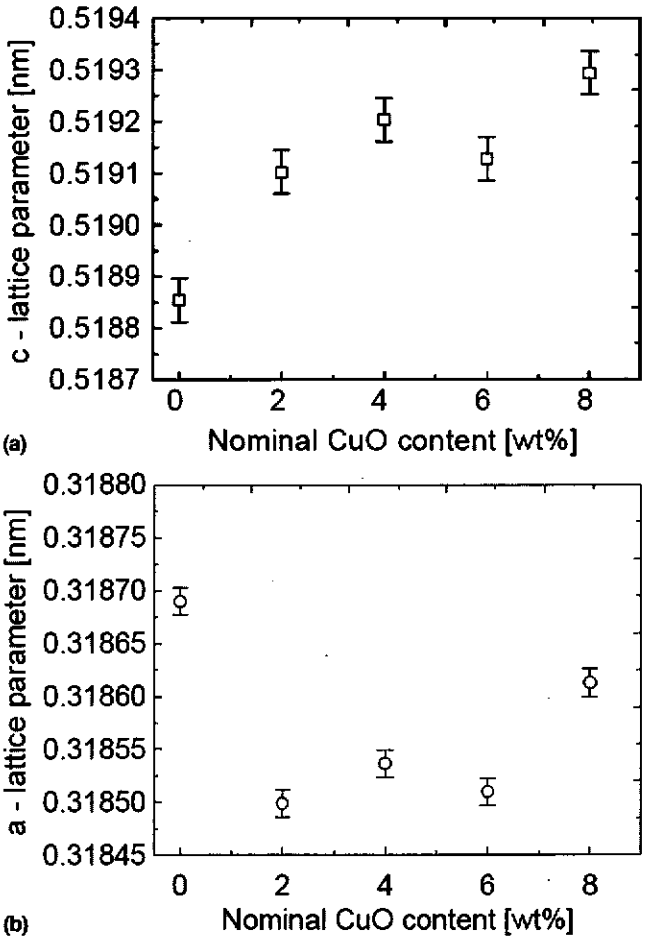

FIG. 5. Average lattice constants of the GaN phases versus nominal CuO content in the samples G0 to G8. (a) *c*-lattice constant and (b) *a*-lattice constants.

From the results of Wahl et al.,[29] it is likely that the copper incorporation takes place primarily on gallium sites. Tetrahedral coordinated copper possesses a larger ionic radius than tetrahedral coordinated gallium (Cu^{2+} 71 pm, Ga^{3+} 61 pm),[39] which would result in an enlargement of the unit cell. A corresponding trend can be seen in Fig. 5(a) for the *c*-lattice constant of the GaN phases in samples G0 to G4 and G6 to G8. For the *a*-lattice constants of the GaN phases of the CuO-calcined samples, G2 to G4 and G6 to G8, a similar trend can be seen in Fig. 5(b).

We do not have an explanation for the observation that the unit cell initially contracts along the *a*-direction for low nominal CuO contents. It is highly speculative to try to explain this behavior with the freed oxygen from the calcination-induced disproportionation of CuO. If one

assumes that oxygen gets incorporated in GaN by replacing nitrogen (which is in agreement with our EELS observations as discussed below), one should observe a contraction of the *a*-lattice constant since the tetrahedral coordinated oxygen anion possesses a smaller radius than the tetrahedral coordinated nitrogen anion (O^{2-} 124 pm, N^{3-} 132 pm).[39] Note that there is essentially no quantitative correlation between the trends in the observed lattice constants, Fig. 5, and the trend in our SQUID measurements, Fig. 1. In addition, there is no qualitative correlation between our lattice parameter changes with nominal CuO content observations, Fig. 5, and the respective theoretical results by Wu and co-workers.[6] (Those authors calculated from first principles the resulting change in the lattice constants of GaN when 6.25 at.% Cu are substitutionally incorporated on Ga sites.[6] In disagreement with our observations, they obtained reductions of –0.15% and –0.19% for both the *a*- and *c*-lattice constants. Wu's and co-workers' calculated lattice parameters for undoped GaN[6] are, however, roughly 2% higher than the generally accepted experimental values.)

By comparing the net shifts of the GaN lattice constants between samples G2 to G8, we find that the relative expansion in the [0001] direction is approximately twice that in the ⟨1000⟩ directions. This is similar to Hern's and co-workers' results for another Cu-doped wurtzite type semiconductor,[40] i.e., a 0.28% increase of the *a*-lattice constants and a 0.68% increase of the *c*-lattice constant when the average unit cell of Cu-doped ZnO is compared with that of undoped ZnO.

Buchholz and co-workers reported that the incorporation of copper barely effects the *a*-lattice constants in the wurtzite (ZnO) structure.[23] Those authors also reported for Cu doping of ZnO a contraction of the unit cell in the [0001] direction (Cu^{2+} possess a smaller ion radius than Zn^{2+}, Ref. 39). Unit-cell dimension changes in the ⟨1000⟩ directions of the wurtzite (ZnO) structure were thought to be due primarily to changes to the anion sites.[23] From our own observations, we conclude that copper incorporation in the GaN phases of our samples leads to an anisotropic expansion of the GaN unit cell and occurs primarily along the [0001] direction.

C. Energy dispersive x-ray spectroscopy

For all CuO-calcined samples, EDXS measurements were conducted on single grains as identified from STEM images. In addition to GaN grains, grains containing copper and oxygen (i.e., copper oxides), and grains of silicon (i.e., grains of the standard added for the quantitative XRD experiments) have been identified by EDXS.

Figure 6 shows a typical STEM image [Fig. 6(a)] and two EDX spectra [Fig. 6(b)] from sample G6. The EDX

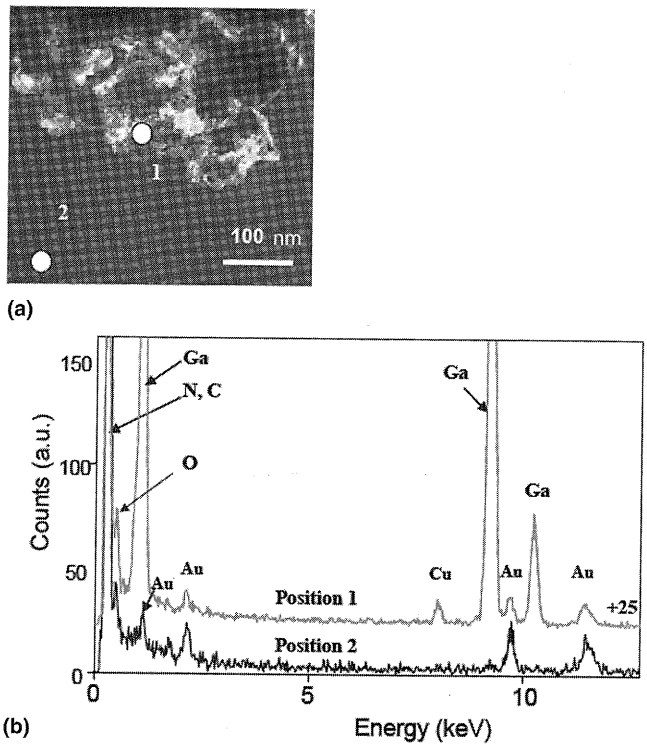

FIG. 6. (a) STEM image from a GaN grain of sample G6. The two positions of the electron beam are circled. (b) EDX spectra of sample G6. At position 1, the strongest peaks belong to nitrogen (N K-edge ~392 eV) and gallium (Ga $L_{1,2}$-edge ~1.1 keV, Ga K_1-edge ~9.24 keV, and Ga K_2-edge ~10.26 keV). Additionally, copper (Cu K_1-edge ~8.04 keV), oxygen (O K-edge ~525 eV) and gold (Au L_1-edge ~9.71 keV, Au L_2-edge ~11.5 keV, and Au $M_{1,2}$-edge ~2.14 keV) were identified. The EDX spectrum of position 2 shows the background signal of the carbon coated gold grid (C K-edge ~277 eV).

spectra were taken at two different positions [Fig. 6(a)], on a GaN grain (position 1) and at an arbitrary location on the carbon film that covers the gold grid to record a local background spectrum (position 2). In the EDX spectrum of the GaN grain [position 1, Fig. 6(b)], Ga, N, Cu, O, and Au peaks are observed. Expectedly, the strongest peaks in Fig. 6(b), position 1, belong to N and Ga. The nitrogen K-edge signal is detected at 392 eV, and the Ga L-edge and Ga K-edge signals are around 200 and 900 eV, respectively. The peak at 8.04 keV [Fig. 6(b), position 1] is determined to be the Cu K-edge. Another peak around 530 eV, the O K-edge, is sitting on the shoulder of the large N K-edge signal (392 eV). Expectedly, using a gold grid in the TEM, several gold peaks are present, Fig. 6(b), position 2. Detecting oxygen in GaN grains is reasonable since oxygen is a frequently occurring impurity in GaN.[41]

Clear copper signals arose in most EDX spectra from individual GaN grains in the CuO-calcined samples. To obtain an estimate of the quantitative copper content in these grains [e.g., Fig. 6(a), position 1], we compared the areas of the K-edges of Cu and Ga and estimated a copper content of a few atomic percent relative to Ga. This

estimate is in reasonable agreement with the solubility of copper in GaN[42] and proves that the spectra were definitely not from copper-oxide grains. (We also confirmed by means of EELS the simultaneous presence of Ga, N, and O in GaN grains that showed a Cu signal in the EDXS.)

D. Electron energy loss spectroscopy

All samples were analyzed by EELS in the STEM mode. Figure 7 shows, for example, an overview core-loss EEL spectrum of a GaN grain of sample G6. Not unexpectedly, the spectrum contains the N K-edge at 405 eV as well as the Ga L_3-edge at 1115 eV. In addition, an oxygen signal (O K-edge at 532 eV) was detected. Apart from Ga and N, an oxygen signal was always present, even in the nominally pure GaN reference sample, G0. As mentioned previously, the presence of oxygen is not surprising since oxygen occurs frequently as an impurity in GaN.[41]

No direct indication of the presence of copper has been found by EELS since the Cu $L_{2,3}$-edge at 931 eV cannot unambiguously be distinguished from the noise in that energy region for any one of our observations. The absence of the Cu signal may be explained by the presumably small amount of Cu in the GaN grains and with the rather small inelastic cross section of the Cu L-excitation. [Using the SIGMAL3 and SIGMAK3 programs,[43] the partial inelastic cross sections of the different excitations can be estimated. For a collection angle of 3 mrad and an energy window of 60 eV, a partial inelastic cross section of the Cu L-excitation of 0.016 pm^2 can be calculated, whereas the partial inelastic cross section of the O K-excitation (0.038 pm^2) and the N K-excitation (0.083 pm^2) are by a factor 2.4 and 5.2 larger.] We conclude, therefore, that the amount of Cu in the GaN grains must be below the detection limit of EELS.

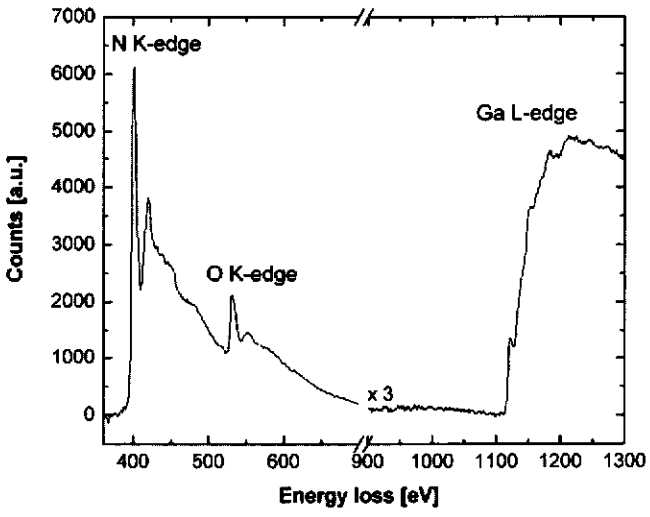

FIG. 7. Overview core-loss EEL spectrum of GaN calcined with 6% CuO, sample G6. The nitrogen K-edge at ~405 eV, the oxygen K-edge at ~532 eV, and the Ga L_3-edge at ~1115 eV are visible. Due to the small concentration of Cu and its small partial inelastic cross section, the Cu $L_{2,3}$ edge (~931 eV) can not be distinguished from the noise in that energy region.

Although direct EELS evidence of the presence of Cu is missing, "two" distinct features were found that reveal the effects of Cu incorporation on the electronic structure of GaN. The "first" feature is found in the fine structure of the N K-edge. Figure 8 compares the N K-edge of GaN grains from samples G0 (nominally pure GaN) and G6 (which was calcined with 6% CuO). Both spectra show four peaks between 405 and 415 eV, labeled A, B, C, and D.

The N K-edge spectrum of the GaN grain from the no-CuO-containing reference sample G0 is in agreement with experimental EELS data of wurtzite GaN.[44] This demonstrates that oxygen impurities, present in all GaN grains investigated, barely affect the fine structure of the N K-edge. Although these four peaks can be identified in GaN of all CuO-calcined samples as well, the relative intensities of the peaks are different, the intensity of peak A is increased, peak C is slightly reduced whereas peaks B and D show similar relative intensities compared to the no-CuO-containing reference sample, G0. The reasons for the change in the peak ratios can be manifold; it could be caused by either (i) the observed change of the lattice constants (c-expansion as observed by XRD), (ii) a change of the chemical bonding or coordination related to a change of the chemical composition (Cu incorporation), or (iii) the crystal orientation dependence of the EELS signal.

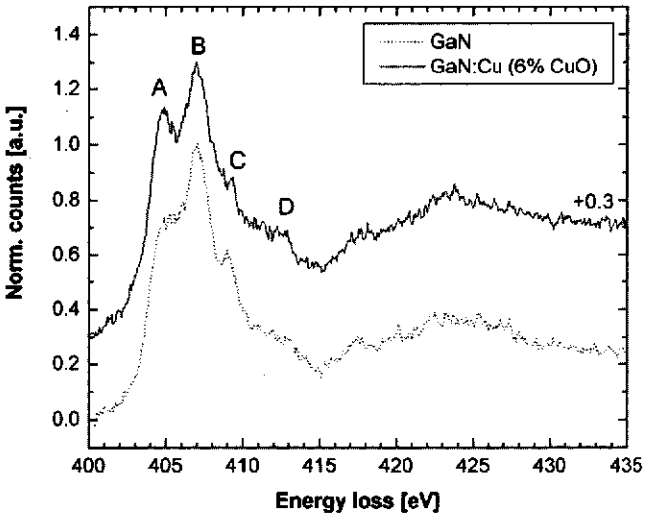

FIG. 8. Fine structure of the nitrogen K-edge of a nominally pure GaN grain (dotted line, sample G0) and a GaN grain that was calcined in the presence of 6% CuO (full line, sample G6). Four distinct peaks, which are labeled A, B, C, and D, between 405 and 415 eV can be identified. Cu incorporation in GaN affects the relative peak intensities. The spectra were recorded with a monochromated electron beam, which allows for energy resolution of ~0.2 to 0.25 eV. Both spectra are the sum of three randomly chosen individual spectra.

Spectra were recorded without determining the actual grain orientation, but always resulted in the same characteristic of the nitrogen K-edge edge in CuO-calcined GaN. In addition, the spectra shown in Fig. 8 are the sum of three randomly chosen N K-edge spectra, which all show the same characteristics. Therefore, it is unlikely that point (iii) mentioned previously, may explain the change in the fine structure of the N K-edge.

Using first-principles calculations, Mizoguchi and co-workers analyzed the relative intensities of peaks A, B, C, and D as a function of the crystal structure of GaN (wurtzite, zinc blende, and rock salt).[45] Those authors found similar spectra for wurtzite and zinc blende GaN. For the rock-salt structure, where the atomic coordination is different, Mizoguchi and co-workers found an increase of peak A while peak D was almost absent.[45] This gives reason to assume that Cu incorporation affects the chemical coordination of nitrogen in GaN.

The "second" EELS feature that reveals the effects of Cu incorporation on the electronic structure of GaN was observed by valence electron energy loss spectroscopy (VEELS). Figure 9 compares a VEEL spectrum from a GaN grain of the no-CuO-containing reference GaN sample, G0, with its counterpart in sample G6 (which was calcined with 6% CuO). A closer inspection of the band gap region of GaN grains of these two samples (see figure inset for convenience) reveals distinct differences between the two spectra. The spectrum from the nominally pure GaN reference sample, G0, shows a band gap signal at ~3.4 eV, which corresponds to the band gap energy of wurtzite GaN.[46] The spectrum of the sample that was calcined with 6% CuO, G6, shows, apart from the actual band-gap signal at ~3.4 eV, a first intensity onset at ~1.7 eV. This suggests that the Cu incorporation gives rise to additional "defect" states (or a defect band) within the GaN band gap.

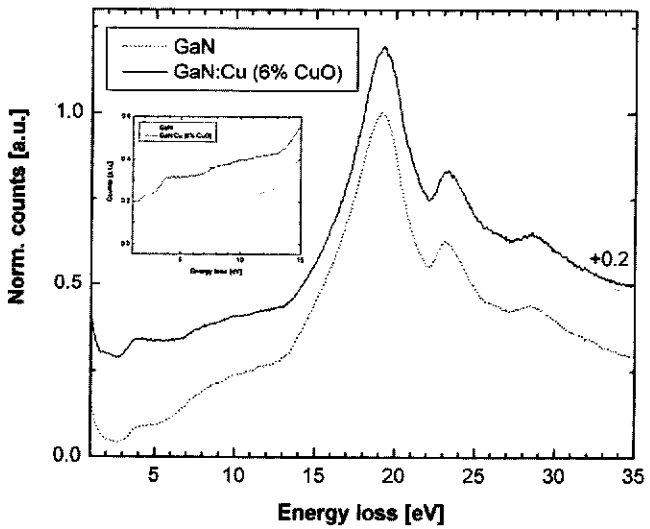

FIG. 9. Valence electron energy loss spectrum of a no-Cu containing GaN reference grain (dotted line, from sample G0) and a CuO-calcined GaN grain (GaN:Cu, full line, from sample G6). Note the shift in the plasmon peak energy from 19.1–19.3 eV that is indicative of calcination-induced changes of the majority-minority electrical carrier concentrations). Inset: Zoom into the band gap region. The no-Cu-containing reference GaN grain (dotted line, sample G0) shows a band gap signal at ~3.4 eV. The CuO-calcined GaN grain (from sample G6) shows in addition to the band gap signal at ~3.4 eV an intensity onset at ~1.7 eV, which reveals that Cu incorporation causes the formation of "defect" states (or a "defect" band) within the actual GaN band gap. (For clarity, the background correction remains of the zero-loss peaks have been removed in the inset.)

IV. SUMMARY AND CONCLUSIONS

Employing independent methods in two different laboratories, we detected room-temperature ferromagnetism in GaN powders that were calcined with CuO. These observations are qualitatively consistent with very recent spin density functional theory calculations by other authors. While we did not elucidate experimentally the exact source of the ferromagnetism, we identified changes in the atomic and electronic structure of GaN that are due to the calcination process.

Anisotropic increases of the lattice constants of GaN were observed. We concluded that this is due to the preferential incorporation of copper along the crystallographic *c*-axis. EDXS confirmed that copper is present in GaN grains. Significant differences in the fine structure of the N K-edge as well as in the valence electron energy loss region of the GaN grains were observed. (The changes in the fine structure of the N K-edge are consistent with an expansion of the *c*-lattice constant of GaN as quantified by XRD.) "Defect states" within the band gap of GaN grains and changes of the chemical bonding and/or the coordination of GaN were observed.

In conclusion, our results demonstrate that ferromagnetic GaN powders have been obtained by our CuO calcination (at 773 K under flowing nitrogen for 4 h) procedure. As far as we know, this paper is (i) the first report on experimentally observed room-temperature ferromagnetism in Cu-doped GaN and (ii) the first report on structural and electronic effects of CuO calcination on GaN powders.

ACKNOWLEDGMENTS

This research was supported by an award from Research Corporation (to P. Moeck). A visiting faculty award from the Lawrence Berkeley National Laboratory (LBNL) (to P. Moeck) supported this research as well. Faculty enhancement and development awards from PSU (to P. Moeck) are also gratefully acknowledged. Research in Sweden was supported by the funding agency VINNOVA (Swedish Governmental Agency for Innovation Systems). The work at LBNL was supported by the

Director, Office of Science, Office of Basic Energy Sciences, of the United States Department of Energy under Contract No. DE-AC03-76SF00098 and under Grant No. DE-FG02-03ER46057. The authors are grateful to Dr. Georg Grathoff (PSU—Geology) and Mrs. Lori Noice (PSU—Physics) for technical assistance with the XRD-measurements and fruitful discussions. A. Gupta is grateful for the hospitality she enjoyed during her stays at both PSU and the LBNL.

REFERENCES

1. S.A. Wolf, D.D. Awschalom, R.A. Buhrman, J.M. Daughton, S. von Molnar, M.L. Roukes, A.Y. Chtchelkanova, and D.M. Treger: Spintronics: A spin-based electronics vision for the future. *Science* **294,** 1488 (2001).
2. I. Zutic, J. Fabian, and S. Das Sarma: Spintronics: Fundamentals and applications. *Rev. Mod. Phys.* **76,** 323 (2004).
3. H. Ohno: Making nonmagnetic semiconductors ferromagnetic. *Science* **281,** 951 (1998).
4. S.A. Chambers: Ferromagnetism in doped thin-film oxide and nitride semiconductors and dielectrics. *Surf. Sci. Rep.* **61,** 345 (2006).
5. T. Dietl, H. Ohno, F. Matsukura, J. Cibert, and D. Ferrand: Zener model description of ferromagnetism in zinc-blende magnetic semiconductors. *Science* **287,** 1019 (2000).
6. R.Q. Wu, G.W. Peng, L. Liu, Y.P. Feng, Z.G. Huang, and Q.Y. Wu: Cu-doped GaN: A dilute magnetic semiconductor from first-principles study. *Appl. Phys. Lett.* **89,** 062505 (2006).
7. P. Sharma, A. Gupta, K.V. Rao, F.J. Owens, R. Sharma, R. Ahuja, J.M.O. Guillen, B. Johansson, and G.A. Gehring: Ferromagnetism above room temperature in bulk and transparent thin films of Mn-doped ZnO. *Nat. Mater.* **2,** 673 (2003).
8. N. Theodoropoulou, V. Misra, J. Philip, P. LeClair, G.P. Berera, J.S. Moodera, B. Satpati, and T. Som: High-temperature ferromagnetism in $Zn_{1-x}Mn_xO$ semiconductor thin films. *J. Magn. Magn. Mat.* **300,** 407 (2006).
9. J.R. Neal, A.J. Behan, R.M. Ibrahim, H.J. Blythe, M. Ziese, A.M. Fox, and G.A. Gehring: Room-temperature magneto-optics of ferromagnetic transition-metal-doped ZnO thin films. *Phys. Rev. Lett.* **96,** 197208 (2006).
10. N.S. Norberg, K.R. Kittilstved, J.E. Amonette, R.K. Kukkadapu, D.A. Schwartz, and D.R. Gamelin: Synthesis of colloidal Mn2+: ZnO quantum dots and high-Tc ferromagnetic nanocrystalline thin films. *J. Am. Chem. Soc.* **126,** 9387 (2004).
11. M.J. Reed, F.E. Arkun, E.A. Berkman, N.A. Elmasry, J. Zavada, M.O. Luen, M.L. Reed, and S.M. Bedair: Effect of doping on the magnetic properties of GaMnN: Fermi level engineering. *Appl. Phys. Lett.* **86,** 102504 (2005).
12. G.T. Thaler, M.E. Overberg, B. Gila, R. Frazier, C.R. Abernathy, S.J. Pearton, J.S. Lee, S.Y. Lee, Y.D. Park, Z.G. Khim, J. Kim, and F. Ren: Magnetic properties of n-GaMnN thin films. *Appl. Phys. Lett.* **80,** 3964 (2002).
13. M.L. Reed, N.A. El-Masry, H.H. Stadelmaier, M.K. Ritums, M.J. Reed, C.A. Parker, J.C. Roberts, and S.M. Bedair: Room temperature ferromagnetic properties of (Ga, Mn)N. *Appl. Phys. Lett.* **79,** 3473 (2001).
14. S.E. Park, H.J. Lee, Y.C. Cho, S.Y. Jeong, C.R. Cho, and S. Cho: Room-temperature ferromagnetism in Cr-doped GaN single crystals. *Appl. Phys. Lett.* **80,** 4187 (2002).
15. S.Y. Han, J. Hite, G.T. Thaler, R.M. Frazier, C.R. Abernathy, S.J. Pearton, H.K. Choi, W.O. Lee, Y.D. Park, J.M. Zavada, and R. Gwilliam: Effect of Gd implantation on the structural and magnetic properties of GaN and AlN. *Appl. Phys. Lett.* **88,** 042102 (2006).
16. P. Sharma, A. Gupta, F.J. Owens, A. Inoue, and K.V. Rao: Room temperature spintronic material—Mn-doped ZnO revisited. *J. Magn. Magn. Mat.* **282,** 115 (2004).
17. K.R. Kittilstved and D.R. Gamelin: Activation of high-T-c ferromagnetism in Mn2+-doped ZnO using amines. *J. Am. Chem. Soc.* **127,** 5292 (2005).
18. M.S. Park and B.I. Min: Ferromagnetism in ZnO co-doped with transition metals: $Zn_{1-x}(FeCo)_xO$ and $Zn_{1-x}(FeCu)_xO$. *Phys. Rev. B* **68,** 224436 (2003).
19. K.R. Kittilstved and D.R. Gamelin: Manipulating polar ferromagnetism in transition-metal-doped ZnO: Why manganese is different from cobalt (invited). *J. Appl. Phys.* **99,** 08M112 (2006).
20. K.R. Kittilstved, W.K. Liu, and D.R. Gamelin: Electronic structure origins of polarity-dependent high-TC ferromagnetism oxide-diluted magnetic semiconductors. *Nat. Mater.* **5,** 291 (2006).
21. O.D. Jayakumar, I.K. Gopalakrishnan, and S.K. Kulshreshtha: The structural and magnetization studies of Co-doped ZnO co-doped with Cu: Synthesized by co-precipitation method. *J. Mater. Chem.* **15,** 3514 (2005).
22. P.V. Radovanovic and D.R. Gamelin: High-temperature ferromagnetism in Ni^{2+}-doped ZnO aggregates prepared from colloidal diluted magnetic semiconductor quantum dots. *Phys. Rev. Lett.* **91,** 157202 (2003).
23. D.B. Buchholz, R.P.H. Chang, J.H. Song, and J.B. Ketterson: Room-temperature ferromagnetism in Cu-doped ZnO thin films. *Appl. Phys. Lett.* **87,** 082504 (2005).
24. A. Gupta: Novel room temperature ferromagnetic semiconductors. Ph.D. Thesis, Department of Materials Science, The Royal Institute of Technology, Stockholm, Sweden, 2004, p. 58.
25. C. Liu, F. Yun, and H. Morkoc: Ferromagnetism of ZnO and GaN: A review. *J. Mater. Sci. Mater. Electron.* **16,** 555 (2005).
26. X.B. Feng: Electronic structures and ferromagnetism of Cu- and Mn-doped ZnO. *J. Phys. Condens. Matter* **16,** 4251 (2004).
27. M. Wei, N. Braddon, D. Zhi, P.A. Midgley, S.K. Chen, M.G. Blamire, and J.L. MacManus-Driscoll: Room temperature ferromagnetism in bulk Mn-doped Cu_2O. *Appl. Phys. Lett.* **86,** 072514 (2005).
28. W.H. Brumage, C.F. Dorman, and C.R. Quade: Temperature-dependent paramagnetic susceptibilities of Cu^{2+} and Co^{2+} as dilute impurities in ZnO. *Phys. Rev. B* **6310,** 104411 (2001).
29. U. Wahl, E. Rita, J.G. Correia, E. Alves, and J.G. Soares: Lattice location and stability of implanted Cu in ZnO. *Phys. Rev. B* **69,** 012102 (2004).
30. P. Bogusławski and J. Bernholc: Properties of wurtzite w-MnN and of w-MnN inclusions in (Ga,Mn)N. *Appl. Phys. Lett.* **88,** 9 (2006).
31. S.J. Pearton, C.R. Abernathy, G.T. Thaler, R.M. Frazier, Y.H. Heo, M. Ivill, D.P. Norton, and Y.D. Park: Progress in wide bandgap ferromagnetic semiconductors and semiconducting oxides, in *Defects and Diffusion in Semiconductors—An Annual Retrospective VII* **230–232,** 520 (2004).
32. S.J. Pearton, C.R. Abernathy, G.T. Thaler, R.M. Frazier, D.P. Norton, F. Ren, Y.D. Park, J.M. Zavada, A. Buyanova, W.M. Chen, and A.F. Hebard: Wide bandgap GaN-based semiconductors for spintronics. *J. Phys. Condens. Matter* **16,** R209 (2004).
33. F.J. Owens: Ferromagnetism above room temperature in bulk sintered gallium phosphide doped with manganese. *J. Phys. Chem. Solids* **66,** 793 (2005).
34. J. Rodriguez-Carvajal: FULLPROF: A Program for Rietveld Refinement and Pattern Matching Analysis, Abstracts of the Satellite Meeting on Powder Diffraction of the XV Congress of the IUCr, Toulouse, France 127, 1990.
35. H.A. Brink, M.M.G. Barfels, R.P. Burgner, and B.N. Edwards: A

sub-50 meV spectrometer and energy filter for use in combination with 200 kV monochromated (S). *TEMs, Ultramicroscopy* **96,** 367 (2003).
36. R. Erni, N.D. Browning, Z.R. Dai, and J.P. Bradley: Analysis of extraterrestrial particles using monochromated electron energy-loss spectroscopy. *Micron* **36,** 369–379 (2005).
37. C. Tiemeijer: Operation modes of a TEM monochromator. *Inst. Phys. Conf. Ser.* **161,** 191 (1999).
38. J.Y. Kim, J.A. Rodriguez, J.C. Hanson, A.I. Frenkel, and P.L. Lee: Reduction of CuO and Cu_2O with H_2: H embedding and kinetic effects in the formation of suboxides. *J. Am. Chem. Soc.* **125,** 10684 (2003).
39. http://abulafia.mt.ic.ac.uk/shannon/: Database of Ionic Radii.
40. T.S. Herng, S.P. Lau, S.F. Yu, H.Y. Yang, X.H. Ji, J.S. Chen, N. Yasui, and H. Inaba: Origin of room temperature ferromagnetism in ZnO: Cu films. *J. Appl. Phys.* **99,** 4212 (2006).
41. T. Mattila and R.M. Nieminen: Ab initio study of oxygen point defects in GaAs, GaN, and AlN. *Phys. Rev. B* **54,** 16676 (1996).
42. Z.W. Jin, T. Fukumura, M. Kawasaki, K. Ando, H. Saito, T. Sekiguchi, Y.Z. Yoo, M. Murakami, Y. Matsumoto, T. Hasegawa, and H. Koinuma: High throughput fabrication of transition-metal-doped epitaxial ZnO thin films: A series of oxide-diluted magnetic semiconductors and their properties. *Appl. Phys. Lett.* **78,** 3824 (2001).
43. R.F. Egerton: Electron energy-loss spectroscopy in the electron microscope, 485 (Plenum Press, New York, 1996).
44. S. Lazar, C. Hebert, and H.W. Zandbergen: Investigation of hexagonal and cubic GaN by high-resolution electron energy-loss spectroscopy and density-functional theory. *Ultramicroscopy* **98,** 249 (2004).
45. T. Mizoguchi, I. Tanaka, S. Yoshioka, M. Kunisu, T. Yamamoto, and W.Y. Ching: First-principles calculations of ELNES and XANES of selected wide-gap materials: Dependence on crystal structure and orientation. *Phys. Rev. B* **70,** 045103 (2004).
46. P. Specht, J.C. Ho, X. Xu, R. Armitage, E.R. Weber, R. Erni, and C. Kisielowski: Band transitions in wurtzite GaN and InN determined by valence electron energy loss spectroscopy. *Solid State Commun.* **135,** 340 (2005).